





Constrained thermalization and topological superconductivity

S. Nulty ^{1,*}, J. Vala ^{1,2}, D. Meidan ³ and G. Kells ²

¹*Department of Theoretical Physics, National University of Ireland, Maynooth, Co. Kildare, Ireland*

²*Dublin Institute for Advanced Studies, School of Theoretical Physics, 10 Burlington Rd, Dublin, Ireland*

³*Department of Physics, Ben-Gurion University of the Negev, Beer-Sheva 84105, Israel*

 (Received 20 March 2020; revised 19 July 2020; accepted 20 July 2020; published 10 August 2020)

We examine the thermalization/localization trade off in an interacting and disordered Kitaev model, specifically addressing whether signatures of many-body localization can coexist with the systems topological phase. Using methods applicable to finite size systems (e.g., the generalized one-particle density matrix, eigenstate entanglement entropy, inverse zero modes coherence length), we identify a regime of parameter space in the vicinity of the noninteracting limit where topological superconductivity survives together with a significant violation of the eigenstate-thermalization hypothesis (ETH) at finite energy densities. We further identify that the coexistence regime features an anomalous behavior of the von Neumann entanglement entropy as a function of disorder strength, which we attribute to competing ETH violation mechanisms. At low disorder, prethermalization like effects that occur due to lack of hybridization between high-energy eigenstates reflect an approximate particle conservation law. In this regime the system tends to thermalize to a generalized Gibbs (as opposed to a grand canonical) ensemble. Moderate disorder tends to drive the system towards stronger hybridization and a standard thermal ensemble, where the approximate conservation law is violated. This behavior is cut off by strong disorder which obstructs many-body effects thus violating ETH and reducing the entanglement entropy.

DOI: [10.1103/PhysRevB.102.054508](https://doi.org/10.1103/PhysRevB.102.054508)

The possibility of realizing Majorana bound states in proximity coupled systems [1–9] has spurred a great deal of activity over the last decade [10–20]. Much of this stems from the belief that quantum devices, based on symmetry protected topological order (SPTO), are a promising platform for quantum information processing as they are robust against many common forms of decoherence [21–25].

With the aspiration of enhancing the stability of these systems at higher temperatures, in recent years there has also been a growing interest in the behavior of these systems at energies well above the topological gap. In this respect, one exciting prospect is that it may be possible for regions of the topological parameter space to coincide with interacting regions that violate the eigenstate-thermalization hypothesis (ETH) [26–28] due to localization in Fock space [29–31]. If this can be engineered, it is expected that systematic errors due to nonadiabatic manipulation (see [32–36]) and/or interaction with the environment (see [37–51]) can be suppressed.

The goal of this paper is to find out if/where the topological-order and many-body localizing behavior overlap in the interacting Kitaev chain (or Kitaev-Hubbard), the prototypical model used to study this effect. One challenging aspect here is that the key parameters being examined, namely disorder [52–59] and interaction strength [60–68], both eventually conspire to drive the system out of the topological phase. On the other hand, these effects work in opposition when considering localization induced violations of ETH and hence, for a given interaction strength, one has to consider

whether the disorder required to prevent thermalization is weak enough to keep the topological properties of the phase intact [31].

Our first result is that there are indeed regions of parameter space where both MBL signatures and topological order can coexist, although these regions can generally only occur in a narrow window about the noninteracting regime. The key result in this regard is the contour plot in Fig. 1, in both disorder and interaction strength. The plot shows that the transition to ETH in the model resembles those obtained in other nontopological models (see, e.g., [69]). However, it also clearly illustrates that the measures of ETH and topological order cut through the parameter space in a very different orientation, showing that in a very literal sense that the phenomena are distinct and orthogonal.

Our second key result concerns competing ETH-violating effects in the model, which results in anomalous entanglement properties at high energies. Specifically, we find that in certain regimes of parameter space, weak amounts of disorder can lead to an *increase* in the averaged entanglement entropy. This property is observed in both the full- and one-body entropies (e.g., those calculated from the single particle density matrix [70–75]). We argue that this unusual behavior is also related to effects observed in the study of so-called many-body zero modes [31,76–88].

This phenomena can be cast in the language of prethermalization where the observed ETH violation at relatively weak disorder is due to an approximate conservation law [89]. This effective conservation means that interactions can drive the system towards different types of thermal ensemble averages in agreement with the general predictions of [90–95].

*Corresponding author: stephen.nulty@mu.ie

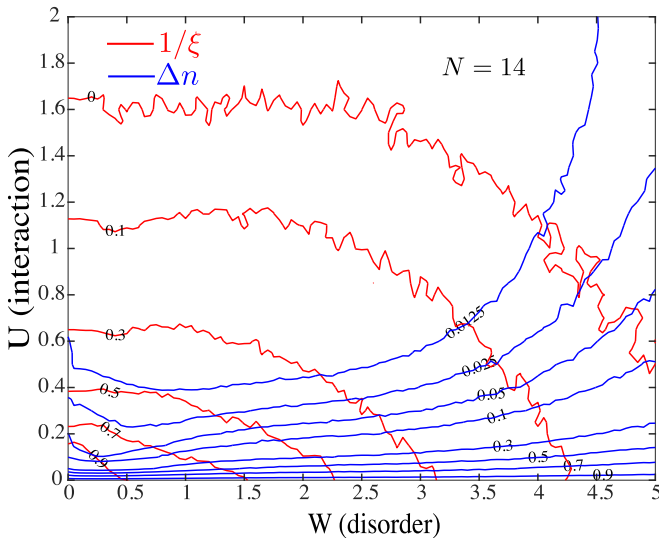


FIG. 1. Average inverse coherence length $\langle 1/\xi \rangle$ (red) and occupation number discontinuity $\langle \Delta n \rangle$ (blue), plotting with increasing disorder strength W and interaction strength U : system size 14 sites, $\mu = 0.4$, $\Delta = 0.7$, 500 disorder realizations. Due to the finite size of the system, one expects $\Delta n \sim O(1/N)$ to be indicative of the ergodic transition, while the edge of the topological region is in principle indicated by values of $\langle 1/\xi \rangle \rightarrow O(1/N)$. The jaggedness of the contours, particularly noticeable at larger disorder strengths, is due to the limited number of disorder realizations available to average the above quantities.

However, we also show that disorder generally degrades this conservation law, and it is this effect that triggers the anomalous entanglement properties. This trend is cut off by strong disorder which violates ETH due to localization effects and leads to a reduction in the entanglement entropy.

I. THE MODEL AND SETUP

We formulate our results via the Kitaev chain model which is a lattice p -wave superconducting model [21]:

$$H_0 = - \sum_{j=1}^N \mu_j \left(c_j^\dagger c_j - \frac{1}{2} \right) - \sum_{j=1}^{N-1} t c_j^\dagger c_{j+1} + \Delta c_j^\dagger c_{j+1}^\dagger + \text{H.c.}, \quad (1)$$

where t is the hopping parameter, Δ is the pairing potential, and μ_j is the local chemical potential at site j . Disorder is introduced by sampling each μ_j uniformly around a mean value μ with the deviation set by a parameter W . Namely, μ_j are uniformly sampled from the interval $[-W + \mu, \mu + W]$. Interactions are introduced by local quartic term giving a density-density type interaction:

$$H_I = 2U \sum_{j=1}^{N-1} \left(c_j^\dagger c_j - \frac{1}{2} \right) \left(c_{j+1}^\dagger c_{j+1} - \frac{1}{2} \right).$$

With U set to zero, the clean model is known to exhibit a topological phase when $|\Delta| > 0$ and $|\mu| < 2t$, with exponentially localized Majorana zero modes at the ends of the wire [21]. In the analysis Δ can be assumed real and in what follows t will be set to one. The goal of our

analysis is to ascertain whether the symmetry protected topological order in this model survives the transition from ETH behavior (eigenstate-thermalization hypothesis [26–28]) to what is known as MBL (many-body localization), see [96].

II. METHODS

To measure the transition from ETH to an MBL-type phase our main tool is a generalization of the occupation gap method [105,106] for superconducting systems that was used previously for this model in [31]. This method has been shown to be a particularly sensitive signature of many-body localization. Given an eigenstate of the Hamiltonian one can construct the generalized single particle density (GSPD) matrix (Appendix A) corresponding to this state, which upon diagonalization, yields so called natural single particle orbitals [105]:

$$\mathcal{R}|\phi_\alpha\rangle = n_\alpha|\phi_\alpha\rangle.$$

In the context of superconductivity or more generally particle nonconserving Hamiltonians, the single particle orbitals will be Bogoliubov quasiparticle orbitals, with eigenvalues n_α that are interpreted as occupations with $0 \leq n_\alpha \leq 1$. The occupation numbers are ordered such that $n_1 \geq n_2 \geq \dots \geq n_{2N}$, and $\text{tr}(\mathcal{R}) = \sum_i n_i = N$.

In the noninteracting limit the numbers $\Delta n = n_N - n_{N+1}$ display a sharp jump from zero to one, delineating empty and filled orbitals. This jump gradually becomes less pronounced as we increase the local interaction strength and move to higher energy densities. In this case introducing disorder tends to on average reduce this trend, reinstating a sharper occupation gap. This gap then offers a means to distinguish ergodic $\Delta n \sim O(1/N)$ from localized $\Delta n \sim O(1)$ phases.

We also probe both full- and one-body entanglement entropies using a base two logarithm in our definition. We perform position space cuts near the center of the wire, of both ground ($\sigma_E = 0$) and high-energy states ($\sigma_E = 1$). For even system sizes this separates sites $\frac{N}{2}$ and $\frac{N}{2} + 1$, while for odd systems sizes this separates sites $\frac{N-1}{2}$ and $\frac{N+1}{2}$. The energy “density” σ_E (denoted ϵ in [106]) is defined as $\sigma_E = 2(E - E_{\min})/(E_{\max} - E_{\min})$, for a given disorder realization. Details on these techniques can be found in Appendix B.

To describe the global trends of entanglement entropy of eigenstates, we compare numerical results to both the thermal (grand canonical) and a generalized Gibbs ensemble defined as

$$\rho_{\text{th}} = \frac{\exp(-\beta H)}{\mathcal{Z}_{\text{th}}}, \quad \rho_G = \frac{\exp(-\beta H - \alpha \mathcal{N})}{\mathcal{Z}_G}, \quad (2)$$

where, for simplicity, H represents the clean ($W = 0$) Kitaev-Hubbard system, and \mathcal{N} is the quasiparticle number operator for the clean noninteracting ($W = U = 0$) model but where we exclude the zero mode number operator. For definition and details on practical implementation see Appendix C.

III. RESULTS

Our key goal is to ascertain if Fock-space localization and topological superconductivity can coexist in this model. To analyze this in Fig. 1 we overlay contour plots of the

values of $\langle \Delta n \rangle$ (in blue) and the inverse effective coherence length $\langle 1/\xi \rangle$ (in red) (also see Appendix D), for a system size $N = 14$. The edge of the topological region is in principle where $\langle 1/\xi \rangle \rightarrow 0$. In practice however, nonexponential decay could be indicated by values of $\langle 1/\xi \rangle \rightarrow O(1/N)$. Similarly for a ETH-MBL boundary in the thermodynamic limit one expects that the occupation gap $\langle \Delta n \rangle$ in ergodic regions to be zero, such that any nonzero value would signal the MBL phase. For finite systems, however, one always expects some small discontinuity and so more realistically the values of $O(1/N)$ should be taken as an indication of the threshold.

In Fig. 1 we see that there is a region of U - W parameter space where the measures for topological and Fock-space localization coexist. One interesting feature is around the chosen parameters ($\mu = 0.4$ and $\Delta = 0.7$) close to the perfectly clean line (y axis), there is a drop in occupation gap if one fixes an interaction strength and increases disorder strength (moving along a horizontal line). This is visible as a dip in the blue occupation gap contours. We will argue below that this is related to a peculiarity in the band structure of this model, which leads to an approximate conservation law that offers some topological protection of high-energy states in the presence of weak interactions [89]. The effect reduces when bands of excited states with different quasiparticle number merge more completely. This occurs for example when one moves to weaker p -wave pairing and/or value of chemical potential that are closer to the bottom of the conduction band. However, as discussed in more detail below, disorder also breaks this approximate conservation. We show below that this explains why introducing small amounts of disorder into the model can actually lead to an increase in the average entanglement entropy.

A. Entanglement structure of coexisting region

In order to further examine the interplay between ETH-violating mechanisms and topological superconductivity, we examine how the entanglement entropy of a bipartition is changed as we increase both the interaction strength U and the disorder parameter W , focusing on both ground state ($\sigma_E = 0$) and excited states ($\sigma_E = 1$). The ground state properties are shown in Figs. 2 and 3(a), where the full- and one-body-entanglement entropy for systems sizes $N = 12, 13, 14$ are calculated in the even parity sector and disorder averaged for $W = 0.1$ (constant W) and $U = 0.1$ (constant U) lines, respectively.

For the ground state properties we see that for a significant region of the disorder parameter space the entanglement entropy remains roughly constant (~ 1 entangled bit), before eventually becoming reduced at around $W = 2$. The lack of scaling is expected for the ground state of a gapped system following an area law in entanglement entropy. In Fig. 3(c) we also plot the quasiparticle entanglement spectrum for the $N = 12$ system, from where we can see how the individual one-body quasiparticle entanglement spectrum values contribute to the total. From Fig. 3(c) (black and dashed red data) we see that the one-body contribution that dominates is a pair of almost zero eigenvalues, which slowly start to gap out as the system becomes more disordered.

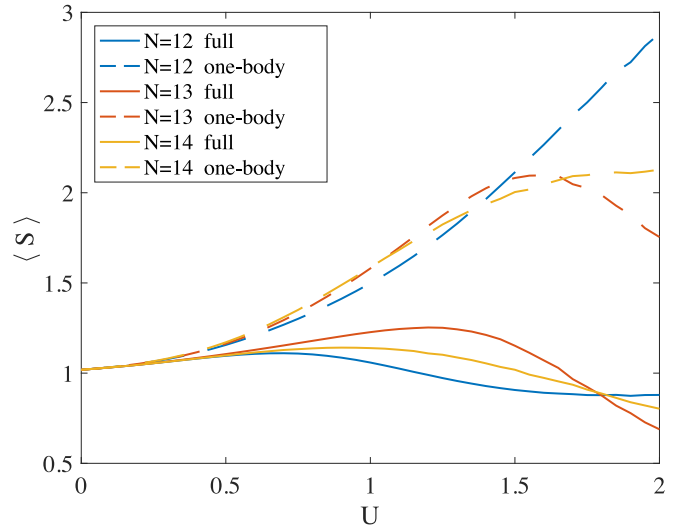


FIG. 2. Entanglement entropies along line $W = 0.1$ for even ground state for sizes $N = 12, 13, 14$, $\mu = 0.4$, $\Delta = 0.7$, 500 realizations. The one-body entanglement entropy (dashed line) tends to be generically higher than the full entanglement entropy (solid line). The difference is minimal however for weakly interacting systems.

For excited states the results are significantly different. First, in Fig. 3(b) we see that the entropy values in low disorder regions are significantly larger than the ground state measures. However, we also see that for these parameter values, modest amounts of disorder actually increase entropy even further before eventually causing it to reduce. The fingerprints of this behavior can also be seen clearly in the quasiparticle entanglement spectrum in Fig. 3(c) (blue data). There we see that the generally higher entropy is caused by an accumulation of the quasiparticle spectrum around the $\varepsilon = 0$ point, where the states contribute the most weight [see, e.g., Fig. 3(d) and Appendix B]. The initial increase in total entropy can be understood as a tightening of this entanglement spectrum band around the $\varepsilon = 0$ line, before eventually dispersing at larger W values. In the next section we will show that this behavior can be understood by examining the relationship between entropy and the many-body spectrum.

B. Entanglement vs energy spectrum: Ensemble switching

While the expected trend is that disorder should decrease the average value of the entanglement entropy, in Fig. 3 we first see an initial increase before the onset of the expected decrease. Similar anomalous behavior can be seen in the lower left corner of Fig. 1 where we see a dip in the blue contours indicating a drop in $\langle \Delta n \rangle$ with disorder. As noted in [106], there is a strong negative correlation between Δn for individual eigenstates and their entanglement entropies. Indeed it was shown that in the ETH phase, eigenstates tend to have large values of entanglement entropy and near-zero values of the occupation gap. In contrast, after the transition to the many-body-localized regime, the occupation gap tends to unity, while the eigenstates have comparatively low values of entropy. The same correlation is shown in Fig. 4, where the averaged entanglement entropy for $\sigma_E = 1$ states has been normalized to lie within the same range as Δn , and is overlaid

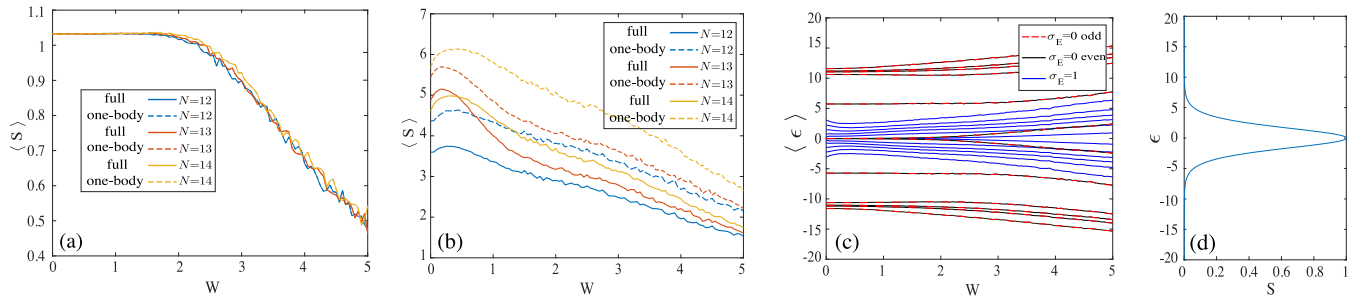


FIG. 3. Half-cut entanglement entropies along line $U = 0.1$ for system sizes $N = 12, 13, 14$, $\mu = 0.4$, $\Delta = 0.7$. (a) Ground state $\sigma_E = 0$ – for the ground states of a weakly interacting system there is minimal difference between the averaged full- and one-body entanglement entropies. (b) Averaged $\sigma_E = 1$ one-body entropy is consistently higher than the full entanglement entropy – the same general trends are observed however. (c) Each mode in the quasiparticle entanglement spectrum contributes to the full entanglement entropy according to (d) [see Eq. (B1)].

with rescaled values of $\langle \Delta n \rangle$ and $1 - \langle \Delta n \rangle$, to show the direct correlation.

In order to pose an explanation for the anomalous increase in entanglement entropy with moderate disorder strength, we study the global properties of entanglement entropy of all eigenstates. The results are plotted in Fig. 5. We identify four distinct behaviors which reflect the interplay between interaction and disorder strength. In particular, we identify regions of parameter space where single particle bands weakly overlap corresponding to relatively weak interaction strength. Here the energy-entropy plots arrange into a pattern of multiple overlapping “parabolas” as shown in Fig. 5(b). This behavior is consistent the von Neumann entropy S of the reduced density matrices of the Gibbs type ρ_G plotted against the expected value of the energy $E = \text{tr}(H\rho_{\text{th/G}})$ as the inverse temperature

β is varied (dashed line), and reflects an approximate particle number conservation law in this regime.

Strong interactions and moderate disorder break this approximate conservation law resulting in a global parabolic trend [Fig. 5(d)]. This is consistent with the von Neumann entropy S of the thermal ensemble ρ_{th} (solid line) and appears in regions of parameter space with negligible occupation number discontinuity (see Fig. 1). Disorder scatters these global structures leading to a reduction in the entanglement entropy which deviates from the thermal or Gibbs ensemble, reflecting the violation of ETH seen in Figs. 5(a) and 5(c).

The anomalous increase in entanglement entropy occurs when crossing from regimes where the behavior is of Gibbs

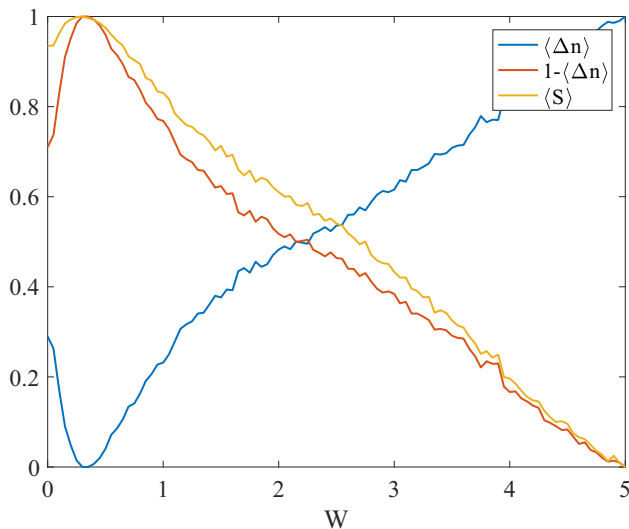


FIG. 4. Normalized entanglement entropy, and occupation gap with increasing disorder strength, for $N = 12$, $\mu = 0.4$, $\Delta = 0.7$, and $U = 0.1$, averaged for 1000 disorder realizations. The normalization is a shift followed by a rescale $x \rightarrow (x - x_{\min}) / (x_{\max} - x_{\min})$, where $x = \langle S \rangle$, $\langle \Delta n \rangle$ and $x_{\max/\min}$ are the max/min values of the averaged quantity along the line $U = 0.1$ with $0 \leq W \leq 5$ as shown in the figure.

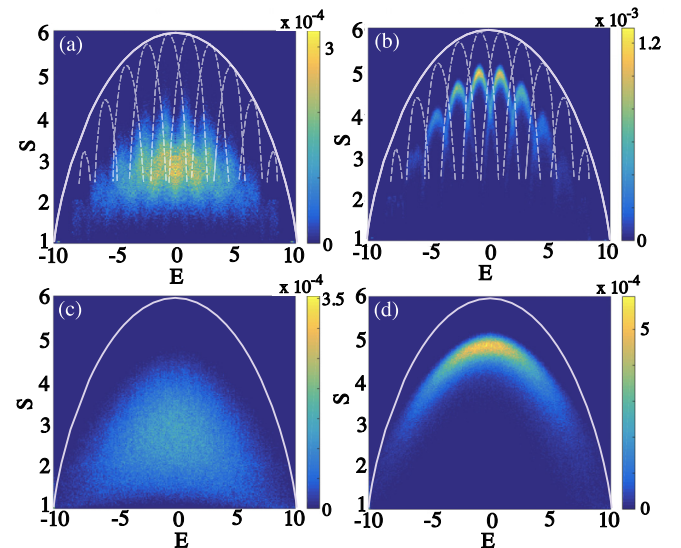


FIG. 5. Entanglement entropy versus energy with $\mu = 0.4$, $\Delta = 0.7$, $N = 12$ sites, for (a) $U = 0.1$, $W = 1$, (b) $U = 0.2$, $W = 0.3$, (c) $U = 0.1$, $W = 2$, and (d) $U = 0.5$, $W = 2$. The solid lines in (a)–(d) represent the von Neumann entropy of the thermal density matrix ρ_{th} as a function of inverse temperature β , while the dashed lines in (a) and (b) represent the von Neumann entropy of the density matrix ρ_G as a function of inverse temperature β , while tuning α to ensure a fixed expected number of quasiparticle excitations. See Eq. (2) and Appendix C.

type [Fig. 5(b)] to regimes approaching the thermal type [Fig. 5(d)]. This behavior is then cut off by a decrease in entanglement entropy caused by increased disorder [Fig. 5(c)]. We note that regions of parameters space characterized by bands that weakly overlap [as in Fig. 5(b)], and thus reflect an approximate particle number conservation, have been shown to protect many-body zero modes [79,80,82,89]. However, here moderate disorder tends to drive the system to regimes where stronger band overlaps occur. This is expected to slightly increase the entanglement entropy and was shown to reduce the topological protection of the many-body zero modes [31]. Stronger disorder then localizes the single particle states and consequently cuts off many-body effects. This is expected to reduce the entanglement entropy and partially restore the protection of the zero modes before eventually driving the system entirely out of the topological phase.

In comparing the peak in the entanglement entropy as a function of disorder in Fig. 3(b), it is noticeable that the width of the peak is visibly smaller for the odd system size compared to the even ones. We note that the average entanglement entropy in Fig. 3(b) is obtained by sampling eigenstates from an energy window centered at energy density $\sigma_E = 1$. For even systems sizes this falls in a valley between overlapping parabolas (close to $E = 0$) similar to Fig. 5(b). For odd system sizes this occurs at the peak of a parabola. This difference together with the observed behavior of the entropy-energy parabolas seem to account for the difference in peak widths, see the Supplemental Material [109].

Here we stress that while this anomalous effect is observed for small values of U and W , where one would expect to observe signatures of the topological phase, the effect itself seems unlikely to be purely topological in nature. For instance, in the Appendix E we examine the model outside of the topological phase, and observe the same increase in entanglement entropy and decrease in Δn for small disorder and weak interactions. In addition, previous studies of global properties of the entanglement entropy in models such as an XXZ ladder, Bose-Hubbard model [107], have shown the same global versus multiparabolic trends when plotting entanglement entropy vs energy.

IV. CONCLUSION

We analyzed the behavior of the disordered Kitaev-Hubbard model with the goal of identifying the coexistence of localization and symmetry protected topological order. Our methodology uses eigenstate entanglement entropy and a generalization of the single particle occupation gap for superconducting systems, and demonstrates that similar to its number conserving counterpart [106], there is a strong correlation between the averaged value of entanglement entropy and the generalized occupation gap for $\sigma_E = 1$ states.

Our analysis allows us to discern distinct mechanisms leading to ETH violation, which can be attributed to prethermalization effects or disorder. In particular, our results identify a narrow region of parameters where SPTO and disorder induced ETH violation can coexist.

In our study we discovered an unexpected increase of the entanglement entropy due to moderate amounts of disorder.

This phenomena occurs when the interacting system transitions between different types of thermal ensembles: The relatively clean system follows a generalized Gibbs-like ensemble with an approximate number conservation law (also known as prethermalization). Moderate disorder shifts the system slightly towards a thermal ensemble, which is eventually cut off by strong disorder, which in turn reduces the entanglement entropy compared to the thermal ensemble.

ACKNOWLEDGMENTS

We are grateful for stimulating conversations with Aaron Conlon, Domenico Pellegrino, Luuk Coopmans, Joost Slingerland, Paul Watts, Shane Dooley, Jiannis Pachos, Fabian Heidrich-Meisner, Masud Haque, and Jens Bardarson. S.N. acknowledges the Government of Ireland Postgraduate Scholarship GOIPG/2014/150 provided by the Irish Research Council. J.V. was funded in part by Science Foundation Ireland under the Principal Investigator Award No. 10/IN.1/I3013. D.M. acknowledges support from the Israel Science Foundation (Grant No. 1884/18). G.K. was supported by a Schrödinger Fellowship and acknowledges support from Science Foundation Ireland through Career Development Award No. 15/CDA/3240.

APPENDIX A: GENERALIZED SINGLE PARTICLE DENSITY MATRIX AND THE OCCUPATION GAP

In Refs. [105,106] it was argued that the discontinuity in the single particle occupation numbers that occurs in noninteracting systems should also persist if the system is in the MBL phase. On the other hand, this occupation gap would be completely washed out in an ergodic (ETH) phase, forming a smooth function in the thermodynamic limit. In order to study the region of overlap between an MBL-type phase and the topological phase of the model we use a generalization of this method to superconducting systems (see, e.g., [31] and references therein). In this method one first forms the generalized single particle density matrix (GSPD herein). Given a fixed number L of fermionic degrees of freedom, and many-body fermionic state Φ , not necessarily an eigenstate of the total number operator \hat{N} , we can form the generalized single particle density matrix \mathcal{R}_Φ by calculating the expectation values of quadratic fermion operators c_i and c_j^\dagger , $1 \leq i, j \leq L$. That is defining the following matrices:

$$\mathcal{R}_\Phi = \begin{pmatrix} \rho & \kappa \\ -\kappa^* & 1 - \rho^* \end{pmatrix}, \quad (\text{A1})$$

where $\rho_{ij} = \langle \Phi | c_j^\dagger c_i | \Phi \rangle$ and $\kappa_{ij} = \langle \Phi | c_j c_i | \Phi \rangle$. This matrix in block form above has the property that it can be used to calculate expectation values in the state Φ of all operators quadratic in the creation and annihilation operators. Writing an operator $\hat{M} = \sum_{i,j} A_{ij} c_i^\dagger c_j + B_{ij} c_i c_j^\dagger + C_{ij} c_i c_j + D_{ij} c_i c_j^\dagger$ in matrix form by collecting the fermi operators in vector form, $\hat{M} = \begin{pmatrix} c^\dagger & c \end{pmatrix} \begin{pmatrix} A & B \\ C & D \end{pmatrix} \begin{pmatrix} c^\dagger \\ c \end{pmatrix}$, $M = \begin{pmatrix} A & B \\ C & D \end{pmatrix}$ then we have that $\langle \Phi | \hat{M} | \Phi \rangle = \text{tr}(\mathcal{R}_\Phi M)$.

Suppose we perform a Bogoliubov transformation of the fermionic operators, $\beta_i^\dagger = \sum_j U_{ji} c_j^\dagger + V_{ji} c_j$, requiring the transformation to be canonical and that $\beta_i = (\beta_i^\dagger)^\dagger$, we find

that the matrix $W = \begin{pmatrix} U & V^* \\ V & U^* \end{pmatrix}$ is unitary, and the transformation can be written as $\begin{pmatrix} \beta \\ \beta^\dagger \end{pmatrix} = W^\dagger \begin{pmatrix} c \\ c^\dagger \end{pmatrix}$. If we form the GSPD matrix of the quasiparticle vacuum state of this transformation, that is the state $|\phi\rangle = \prod \beta_i |0\rangle$, then matrix can be calculated as $\mathcal{R}_\phi = \begin{pmatrix} V^* & \\ & U^* \end{pmatrix} \begin{pmatrix} V^T & \\ & U^T \end{pmatrix}$. In changing to the quasiparticle basis, GSPD matrix of the vacuum state can be put in its canonical form:

$$\mathcal{R}'_\phi = W^\dagger \mathcal{R}_\phi W = \begin{pmatrix} 0 & 0 \\ 0 & 1 \end{pmatrix} = \begin{pmatrix} \langle \phi | \beta^\dagger \beta | \phi \rangle & \langle \phi | \beta \beta | \phi \rangle \\ \langle \phi | \beta^\dagger \beta^\dagger | \phi \rangle & \langle \phi | \beta \beta^\dagger | \phi \rangle \end{pmatrix},$$

from which it is clear that the matrix satisfies $\mathcal{R}'_\phi = \mathcal{R}_\phi$.

APPENDIX B: FULL- AND ONE-BODY ENTANGLEMENT ENTROPIES

To further probe the region of overlap between MBL-type and topological phases of the model, we look at the full- and one-body entanglement entropies, performing position space cuts near the center of the wire, of both ground ($\sigma_E = 0$) and high-energy states ($\sigma_E = 1$). The energy density σ_E (denoted ϵ in [106]) is defined as $\sigma_E = 2(E - E_{\min}) / (E_{\max} - E_{\min})$, for a given disorder realization.

One expects, due to the spatial localization of the many-body wave functions, that the entanglement entropy in an MBL phase to be generally lower than in the ergodic phase. Moreover, it can be shown that one of the defining features of the MBL phase is an area law scaling for entanglement entropy which, for one-dimensional systems, should be constant, or at least bounded by a constant [29,97]. The (generalized) one-body approximation to the entanglement entropy is calculated directly from the reduced (generalized) single particle density matrix. For more details see Appendix A. In the case of free fermion systems this calculation agrees exactly with the standard entanglement entropy (see [70–75]). As one moves to more interacting regimes the one-body entropy generically overestimates the full entropy (see Figs. 2 and 3), although for modest interaction strengths the results are very similar.

Our main motivation for examining the one-body entropy is that it allows us to break down the total entanglement entropy into the contributions from the individual modes of the so-called entanglement Hamiltonian.

For the analysis of the single particle entanglement we will also need to define a reduced density matrix $\tilde{\mathcal{R}}$ where we only consider a subset of matrix indices, corresponding to a partition of the sites in position space. Choosing a subset of the labels (sites) of the fermion operators $\{j_1 \cdots j_k\}$ we can form a reduced density matrix \tilde{R}_ψ by taking only the matrix entries of R_ψ corresponding to the indices $\{j_1 \cdots j_k\}$, which are the expectation values $\langle \psi | c_{j_i}^\dagger c_{j_m} | \psi \rangle$, with $1 \leq i, m \leq k$. This is equivalent to deleting rows and columns for labels (sites) that are to be traced out. Now if one takes the von Neumann entropy of this reduced density matrix, we call this the one-body entanglement entropy $S_{\text{one}} = -\text{tr}[\tilde{R}_\psi \log_2(\tilde{R}_\psi)]$.

It was shown by [70] that this is precisely the entanglement entropy provided that the state is a free fermion eigenstate. In this case we can write $\tilde{\mathcal{R}} = [1 + \exp(H_\alpha)]^{-1}$ [108], where H_α is free fermion single particle/excitation Hamiltonian. Given

that the eigenvalues of $\tilde{\mathcal{R}}$ come in pairs $\frac{1}{2} \pm \eta_i$ due to particle hole symmetry, this means the eigenvalues of H_α come in pairs $\pm \epsilon_i$. The values ϵ_i themselves are known as the quasiparticle entanglement spectrum [75], which generate the entanglement spectrum. Concretely in this case we have

$$S = - \sum_{\epsilon_i > 0} f(\epsilon_i) \log_2[f(\epsilon_i)] + f(-\epsilon_i) \log_2[f(-\epsilon_i)], \quad (\text{B1})$$

where $f(\epsilon) = (1 + e^\epsilon)^{-1}$ and the values $f(\epsilon_i)$ are the eigenvalues of the reduced generalized density matrix $\tilde{\mathcal{R}}$ where the subset are the position space indices for half of the wire (e.g., $j \leq N/2$) [75]. While this function is not symmetric with respect to ϵ , given that the quasiparticle entanglement spectrum is particle hole symmetric, we can combine the positive and negative pairs into a symmetric contribution which peaks at $\epsilon = 0$ as in Eq. (B1).

For a generic state with a definite fermion number parity the one-particle entropy tends to overestimate the entanglement entropy. This is clearly seen in particular in Fig. 3 where even for small interaction strengths the average value for $\sigma_E = 1$ states is approximately one e-bit above the actual value of the entanglement entropy. That said, it is also clear that for the $\sigma_E = 0$ states, even for modest interactions, that the value of the one-body entropy reasonably estimates the actual value of the entanglement entropy. Furthermore, the one-body entropy tends to mimic the global trends in the entropy seen in Fig. 5.

APPENDIX C: THERMAL AND GENERALIZED GIBBS ENSEMBLES

To study the expected MBL and ETH phases of the model we compare numerical results to both the thermal (grand canonical) and a generalized Gibbs ensemble defined as

$$\rho_{\text{th}} = \frac{\exp(-\beta H)}{\mathcal{Z}_{\text{th}}}, \quad (\text{C1})$$

$$\rho_{\text{G}} = \frac{\exp(-\beta H - \alpha \mathcal{N})}{\mathcal{Z}_{\text{G}}}, \quad (\text{C2})$$

where, for simplicity, H represents the clean ($W = 0$) Kitaev-Hubbard system, and \mathcal{N} is the quasiparticle number operator for the clean noninteracting ($W = U = 0$) model but where we exclude the zero mode number operator. To elaborate on the definition of the \mathcal{N} operator, we take the clean ($W = 0$) Kitaev model, diagonalizing as usual with a Bogoliubov transformation so that $H_0 = \sum_j E_j \beta_j^\dagger \beta_j + \Lambda$, Λ being the ground state energy. In the topological phase there are (approximate) zero modes which are combined into a fermion degree of freedom with single particle energy $E_k \sim 0$ for some index k , then \mathcal{N} is simply

$$\mathcal{N} = \sum_{j \neq k} \beta_j^\dagger \beta_j. \quad (\text{C3})$$

With weak disorder and interactions, the energy spectrum maintains the approximate doubling of degeneracy with number parity. Inclusion of the zero mode number operator does not allow the assignment of a single number of quasiparticle excitations to a single band as in Fig. 4(b) (main text), since occupying the zero mode degrees of freedom counts as a

quasiparticle with approximately the same energy. If one includes the zero mode, one sees curves as in Fig. 4(b) (dashed line) which instead encompass two neighboring “parabolas” instead of just one. Here α plays the role of the quasiparticle chemical potential [90–95]. In the thermodynamic limit [97] one expects that if ETH holds, then for a small subsystem A with environment B the reduced density matrix of an eigenstate will agree with the reduced density matrix of $\rho_{\text{th},A} = \text{tr}_B(\rho_{\text{th}})$, with β fixed to give the expected energy of the eigenstate. In particular, this means that the von Neumann entropy of $\rho_{\text{th},A}$ will agree with the entanglement entropy of the eigenstate.

To examine the global trends of entanglement entropy of eigenstates, we study the von Neumann entropy of the reduced thermal matrix $\rho_{\text{th},A}$ as a function of inverse temperature (β). Suppose we partition the wire into subsystems A and B , the environment for a given number of sites N . If one takes the thermodynamic limit, adding degrees of freedom (sites) to the environment B in such a way that the limit of the fraction of sites in A to B goes to zero, then if the ETH holds, subsystem A should be in thermal equilibrium. That is to say if one takes an eigenstate $|\psi_n\rangle$ with energy E_n , and the thermal density matrix for the full system $\rho^{(\text{eq})}(T) = \mathcal{Z}^{-1}(T) \exp(-H/k_B T)$, then

$$\rho_A^{(n)} = \rho_A^{(\text{eq})}(T_n),$$

where $\rho_A^{(n)} = \text{tr}_B(|\psi_n\rangle\langle\psi_n|)$, $\rho_A^{(\text{eq})}(T_n) = \text{tr}_B[\rho^{(\text{eq})}(T_n)]$, and T_n is such that $\text{tr}[H\rho^{(\text{eq})}(T_n)] = E_n$. As noted in [97], this implies that the entropy of entanglement $S_{AB} = -k_B \text{tr}_A \rho_A^{(n)} \log_2 \rho_A^{(n)}$ between A and B for this eigenstate is equal to the equilibrium thermal entropy (von Neumann entropy) of the smaller subsystem, A in this case.

For a fixed chain length, the infinite temperature limit $\beta = 0$, corresponds to $\rho_{\text{th}} = \mathbb{I}/2^N$, the normalized identity operator, which gives $E_{\text{avg}} = \text{tr}(H)/2^N$ for the expected energy, and the von Neumann entropy of the reduced density matrix $\rho_{\text{th},A}$ peaks at $\log_2(D_A)$ where D_A is dimension of reduced Hilbert space of subsystem A . If we allow for negative temperatures, we can compare this to the entanglement entropy of the eigenstates across all energies E , where $E < E_{\text{avg}}$ corresponds to positive temperatures, and $E > E_{\text{avg}}$ corresponds to negative temperatures.

In order to describe trends in the entropy energy of eigenstates, which in the weakly interacting chain still have a near integer expected number of quasiparticles, we also compare against the von Neumann entropy of the reduced Gibbs-type density matrix $\rho_{G,A}$ as a function of inverse temperature. We impose the constraint $n = \text{tr}(\mathcal{N}\rho_G)$, with n an integer $0 \leq n \leq N - 1$. The Gibbs-type operator is the one which maximizes the statistical entropy given this constraint, which is normally arrived at by treating α as a Lagrange multiplier. The trace condition fixes $\alpha(\beta, n)$ as a function of β , and quasiparticle number n . Numerically, however, we would like to find such an α to construct the density matrix, so for fixed values β, n we employ a bisection method on the parameter α .

APPENDIX D: INTERACTION AND TOPOLOGICAL PHASE TRANSITIONS FOR FINITE SYSTEMS

It is known that topological superconductivity survives for a range of disorder and interaction parameters [52–68]. In or-

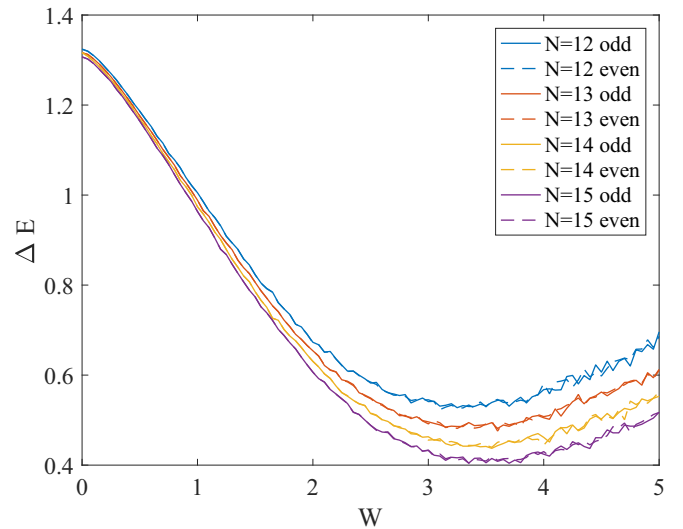


FIG. 6. Energy gap for both number parity sectors as a function of disorder strength with fixed interaction strength $U = 0.1$, $\mu = 0.4$, $\Delta = 0.7$ with 2000 disorder realizations.

der to define the topological phase of the model, one indicator is the gap. Another distinguishing feature is the presence of Majorana modes localized at the ends of the one-dimensional wire. Addressing the first, in Fig. 6 the disorder averaged energy gap to the first excited state in the even/odd parity sector is plotted against disorder and interaction strength.

A clear energy gap can be seen in this figure, and it is expected that the gap closes as interaction strength and/or disorder is increased. It is unlikely that zero will actually be obtained from this disorder averaging process given that the energy gap is calculated as a positive quantity, and averaging at best can yield a small but nonzero number. In order to show the expected closing of the energy gap, in Fig. 6 the even/odd parity energy gap is plotted for increasing system size for a fixed interaction strength $U = 0.1$ which is averaged over 500 disorder realizations. One can see the downward trend of the value of the gap at larger disorder and increasing system size.

In the main text we instead use the inverse of the effective Majorana coherence length $1/\xi$ for the zero modes in the topological phase of the model. Given the (even and odd parity ground states) ground state and first excited state, denoted $|0\rangle$ and $|1\rangle$ of the above model, we define the cross correlators

$$\langle 0|c_j|1\rangle + \langle 0|c_j^\dagger|1\rangle = \langle 0|\gamma_j|1\rangle \quad \text{for } j = 1, \dots, N. \quad (\text{D1})$$

This function of position (j) decays exponentially into the middle of the wire as $e^{-x/\xi}$ where $x = j$ (or $N - j$ if using a minus sign in the definition above). The effective inverse coherence length $1/\xi$ is estimated by taking the logarithm of absolute value of the cross correlators, averaging over disorder realizations, and then performing a linear fit (least squares) from sites 1 up to $\lfloor N/2 \rfloor$. Performing the linear fits first and then averaging over the disorder realizations gives an identical answer, which is a property of linear fitting with the least squares method.

The inverse coherence length is shown in Fig. 7, averaged over 2000 disorder realizations for parameters $U/t = 0.1$, $\mu/t = 0.4$, and $\Delta/t = 0.7$. The coherence length decays

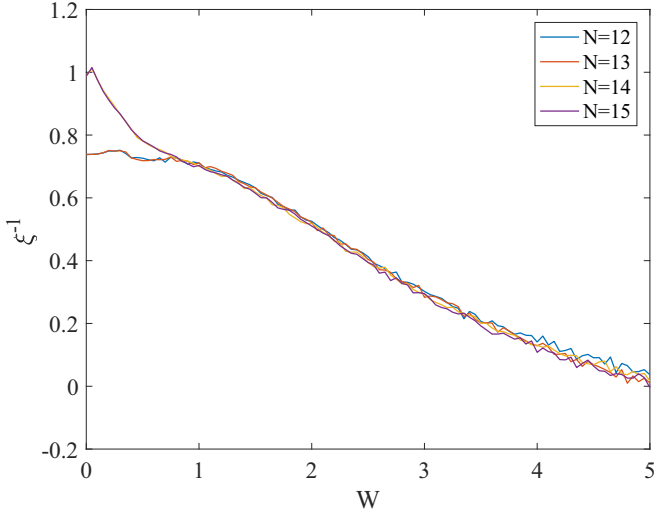


FIG. 7. Inverse coherence length as a function of disorder strength and fixed interaction strength $U = 0.1$, $\mu = 0.4$, $\Delta = 0.7$ with 2000 disorder realizations

to zero relatively consistently when the disorder strength reaches approximately $W \sim 5$. The sudden jump in coherence length from sizes 12,13 to 14,15 is an artificial artifact of the procedure to estimate the coherence length.

APPENDIX E: ENTANGLEMENT ENTROPY AND OCCUPATION GAP

As mentioned in the main text, there is a correlation between the averaged entanglement entropy of eigenstates at $\sigma_E = 0$ and the averaged occupation gap calculated from the GSPD matrix of these eigenstates. In the main text, weak disorder first led to an increase in the averaged entanglement entropy and corresponding decrease in averaged occupation gap. For larger disorder strengths, an overall expected de-

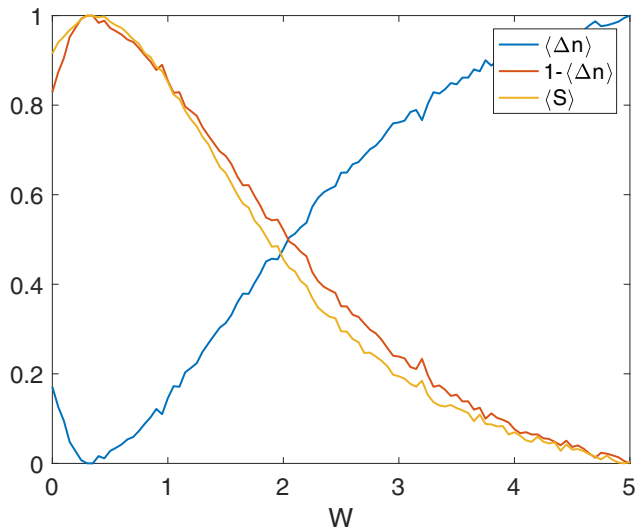


FIG. 8. $N = 13$ sites, $\mu = -3$, $\Delta = 0.7$, $U = 0.1$, 500 disorder realizations. (a) Scaled entanglement entropy and Δn vs disorder strength.

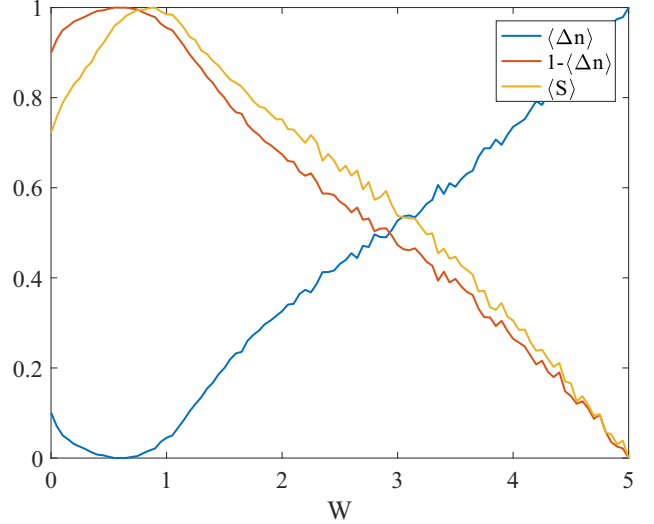


FIG. 9. $N = 13$ sites, $\mu = -0.2$, $\Delta = 0.7$, $U = 0.1$, 500 disorder realizations. (a) Scaled entanglement entropy and Δn vs disorder strength, periodic boundary conditions.

crease in entanglement entropy is seen with its corresponding increase in averaged occupation gap. This was shown starting from a region of parameter space wherein the model is in a topological phase with weak disorder. This increase in averaged entanglement entropy is also noticed in parameter regimes where the model would not be in a topological phase with weak disorder (Fig. 8), and with periodic boundary conditions (Fig. 9). The correlation between averaged entanglement entropy and averaged occupation gap is seen in both cases. The data as in the main text are normalized in Figs. 8 and 9. The normalization is a shift followed by a rescale $x \rightarrow (x - x_{\min}) / (x_{\max} - x_{\min})$, where, $x = \langle S \rangle$, $\langle \Delta n \rangle$ and $x_{\max/\min}$ are the max/min values of the averaged quantity along the line $U = 0.1$ with $0 \leq W \leq 5$ as shown in the figures. It

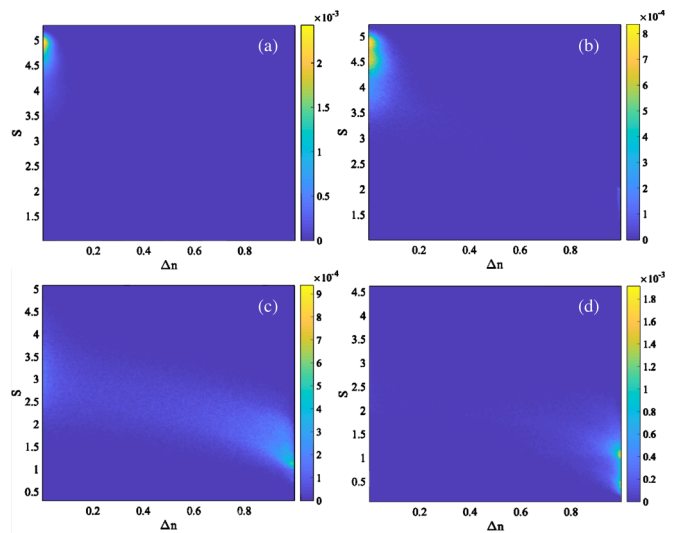


FIG. 10. $N = 12$ sites. Entanglement entropy versus occupation gap for $\mu = 0.4$ and $\Delta = 0.7$ for (a) $U = 0.5$, $W = 0.5$, (b) $U = 0.2$, $W = 0.3$, (c) $U = 0.1$, $W = 3$, and (d) $U = 0.1$, $W = 5$

was noticed in [106] that in the ergodic phase eigenstates with a large half-cut, entanglement entropy tended to have low occupation discontinuity, while in the MBL phase states, eigenstates typically had much lower values of entanglement entropy and higher occupation gaps. This bunching in an entropy-occupation gap plot is also seen in the model of the main text, the Kitaev model with nearest neighbor interac-

tions. In Fig. 10 we show a density plot of the entanglement entropy vs the occupation gap for all eigenstates of the Kitaev model with 100 disorder realizations. We see a bunching of high entropy states with low occupation gap in Figs. 10(a) and 10(b), while in the limit of large disorder Figs. 10(c) and 10(d) states tend to bunch up at lower entropies and have large occupation gaps.

-
- [1] L. Fu and C. L. Kane, Superconducting Proximity Effect and Majorana Fermions at the Surface of a Topological Insulator, *Phys. Rev. Lett.* **100**, 096407 (2008).
 - [2] R. M. Lutchyn, J. D. Sau, and S. Das Sarma, Majorana Fermions and a Topological Phase Transition in Semiconductor-Superconductor Heterostructures, *Phys. Rev. Lett.* **105**, 077001 (2010).
 - [3] Y. Oreg, G. Refael, and F. von Oppen, Helical Liquids and Majorana Bound States in Quantum Wires, *Phys. Rev. Lett.* **105**, 177002 (2010).
 - [4] M. Duckheim and P. W. Brouwer, Andreev reflection from noncentrosymmetric superconductors and Majorana bound-state generation in half-metallic ferromagnets, *Phys. Rev. B* **83**, 054513 (2011).
 - [5] S. B. Chung, H. J. Zhang, X. L. Qi, and S. C. Zhang, Topological superconducting phase and Majorana fermions in half-metal/superconductor heterostructures, *Phys. Rev. B* **84**, 060510(R) (2011).
 - [6] T.-P. Choy, J. M. Edge, A. R. Akhmerov, and C. W. J. Beenakker, Majorana fermions emerging from magnetic nanoparticles on a superconductor without spin-orbit coupling, *Phys. Rev. B* **84**, 195442 (2011).
 - [7] M. Kjaergaard, K. Wölms, and K. Flensberg, Majorana fermions in superconducting nanowires without spin-orbit coupling, *Phys. Rev. B* **85**, 020503(R) (2012).
 - [8] I. Martin and A. F. Morpurgo, Majorana fermions in superconducting helical magnets, *Phys. Rev. B* **85**, 144505 (2012).
 - [9] S. Nadj-Perge, I. K. Drozdov, B. A. Bernevig, and A. Yazdani, Proposal for realizing Majorana fermions in chains of magnetic atoms on a superconductor, *Phys. Rev. B* **88**, 020407(R) (2013).
 - [10] V. Mourik, K. Zuo, S. M. Frolov, S. R. Plissard, E. P. A. M. Bakkers, and L. P. Kouwenhoven, Signatures of Majorana fermions in hybrid superconductor-semiconductor nanowire devices, *Science* **336**, 1003 (2012).
 - [11] M. T. Deng, C. L. Yu, G. Y. Huang, M. Larsson, P. Caroff, and H. Q. Xu, Anomalous zero-bias conductance peak in a Nb-InSb nanowire-Nb hybrid device, *Nano Lett.* **12**, 6414 (2012).
 - [12] A. Das, Y. Ronen, Y. Most, Y. Oreg, M. Heiblum, and H. Shtrikman, Zero-bias peaks and splitting in an Al-InAs nanowire topological superconductor as a signature of Majorana fermions, *Nat. Phys.* **8**, 887 (2012).
 - [13] A. D. K. Finck, D. J. Van Harlingen, P. K. Mohseni, K. Jung, and X. Li, Anomalous Modulation of a Zero-Bias Peak in a Hybrid Nanowire-Superconductor Device, *Phys. Rev. Lett.* **110**, 126406 (2013).
 - [14] H. O. H. Churchill, V. Fatemi, K. Grove-Rasmussen, M. T. Deng, P. Caroff, H. Q. Xu, and C. M. Marcus, Superconductor—nanowire devices from tunneling to the multichannel regime: Zero-bias oscillations and magnetoconductance crossover, *Phys. Rev. B* **87**, 241401(R) (2013).
 - [15] S. M. Albrecht, A. P. Higginbotham, M. Madsen, F. Kuemmeth, T. S. Jespersen, J. Nygård, P. Krogstrup, and C. M. Marcus, Exponential protection of zero modes in Majorana islands, *Nature (London)* **531**, 206 (2016).
 - [16] Ö. Gül, H. Zhang, J. D. S. Bommer, M. W. A. de Moor, D. Car, S. R. Plissard, E. P. A. M. Bakkers, A. Geresdi, K. Watanabe, T. Taniguchi, and L. P. Kouwenhoven, Ballistic Majorana nanowire devices, *Nat. Nanotechnol.* **13**, 192 (2018).
 - [17] M. T. Deng, S. Vaitiekėnas, E. B. Hansen, J. Danon, M. Leijnse, K. Flensberg, J. Nygård, P. Krogstrup, and C. M. Marcus, Majorana bound state in a coupled quantum-dot hybrid-nanowire system, *Science* **354**, 1557 (2016).
 - [18] S. Nadj-Perge, I. K. Drozdov, J. Li, H. Chen, S. Jeon, J. Seo, A. H. MacDonald, B. A. Bernevig, and A. Yazdani, Observation of Majorana fermions in ferromagnetic atomic chains on a superconductor, *Science* **346**, 602 (2014).
 - [19] M. Ruby, F. Pientka, Y. Peng, F. von Oppen, B. W. Heinrich, and K. J. Franke, End States and Subgap Structure in Proximity-Coupled Chains of Magnetic Adatoms, *Phys. Rev. Lett.* **115**, 197204 (2015).
 - [20] R. Pawlak, M. Kisiel, J. Klinovaja, T. Meier, S. Kawai, T. Glatzel, D. Loss, and E. Meyer, Probing atomic structure and Majorana wavefunctions in mono-atomic Fe chains on superconducting Pb surface, *Npj Quantum Inf.* **2**, 16035 (2016).
 - [21] A. Y. Kitaev, Unpaired Majorana fermions in quantum wires, *Phys. Usp.* **44**, 131 (2001).
 - [22] A. Y. Kitaev, Fault-tolerant quantum computation by anyons, *Ann. Phys. (NY)* **303**, 2 (2003).
 - [23] A. Y. Kitaev, Anyons in an exactly solved model and beyond, *Ann. Phys. (NY)* **321**, 2 (2006).
 - [24] C. Nayak, S. H. Simon, A. Stern, M. Freedman, and S. Das Sarma, Non-Abelian anyons and topological quantum computation, *Rev. Mod. Phys.* **80**, 1083 (2008).
 - [25] T. D. Stanescu, *Introduction to Topological Quantum Matter & Quantum Computation* (CRC, Boca Raton, FL, 2016).
 - [26] J. M. Deutsch, Quantum statistical mechanics in a closed system, *Phys. Rev. A* **43**, 2046 (1991).
 - [27] M. Srednicki, Chaos and quantum thermalization, *Phys. Rev. E* **50**, 888 (1994).
 - [28] H. Tasaki, From Quantum Dynamics to the Canonical Distribution: General Picture and a Rigorous Example, *Phys. Rev. Lett.* **80**, 1373 (1998).
 - [29] B. Bauer and C. Nayak, Area laws in a many-body localized state and its implications for topological order, *J. Stat. Mech.* **2013** (2013)P09005.
 - [30] D. A. Huse, R. Nandkishore, V. Oganesyan, A. Pal, and S. L. Sondhi, Localization-protected quantum order, *Phys. Rev. B* **88**, 014206 (2013).
 - [31] G. Kells, N. Moran, and D. Meidan, Localization enhanced and degraded topological order in interacting *p*-wave wires, *Phys. Rev. B* **97**, 085425 (2018).

- [32] M. Cheng, V. Galitski, and S. Das Sarma, Nonadiabatic effects in the braiding of non-Abelian anyons in topological superconductors, *Phys. Rev. B* **84**, 104529 (2011).
- [33] M. S. Scheurer and A. Shnirman, Nonadiabatic processes in Majorana qubit systems, *Phys. Rev. B* **88**, 064515 (2013).
- [34] E. Perfetto, Dynamical Formation and Manipulation of Majorana Fermions in Driven Quantum Wires in Contact with a Superconductor, *Phys. Rev. Lett.* **110**, 087001 (2013).
- [35] B. Bauer, T. Karzig, R. V. Mishmash, A. E. Antipov, and J. Alicea, Dynamics of Majorana-based qubits operated with an array of tunable gates, *SciPost Phys.* **5**, 004 (2018).
- [36] A. Conlon, D. Pellegrino, J. K. Slingerland, S. Dooley, and G. Kells, Error generation and propagation in Majorana based topological qubits, *Phys. Rev. B* **100**, 134307 (2019).
- [37] G. Goldstein and C. Chamon, Decay rates for topological memories encoded with Majorana fermions, *Phys. Rev. B* **84**, 205109 (2011).
- [38] J. C. Budich, S. Walter, and B. Trauzettel, Failure of protection of Majorana based qubits against decoherence, *Phys. Rev. B* **85**, 121405(R) (2012).
- [39] D. Rainis and D. Loss, Majorana qubit decoherence by quasiparticle poisoning, *Phys. Rev. B* **85**, 174533 (2012).
- [40] M. Cheng, R. M. Lutchyn, and S. Das Sarma, Topological protection of Majorana qubits, *Phys. Rev. B* **85**, 165124 (2012).
- [41] M. J. Schmidt, D. Rainis, and D. Loss, Decoherence of Majorana qubits by noisy gates, *Phys. Rev. B* **86**, 085414 (2012).
- [42] F. Konschelle and F. Hassler, Effects of nonequilibrium noise on a quantum memory encoded in Majorana zero modes, *Phys. Rev. B* **88**, 075431 (2013).
- [43] L. Mazza, M. Rizzi, M. D. Lukin, and J. I. Cirac, Robustness of quantum memories based on Majorana zero modes, *Phys. Rev. B* **88**, 205142 (2013).
- [44] S.-H. Ho, S.-P. Chao, C.-H. Chou, and F.-L. Lin, Decoherence patterns of topological qubits from Majorana modes, *New J. Phys.* **16**, 113062 (2014).
- [45] H. T. Ng, Decoherence of interacting Majorana modes, *Sci. Rep.* **5**, 12530 (2015).
- [46] F. L. Pedrocchi and D. P. DiVincenzo, Majorana Braiding with Thermal Noise, *Phys. Rev. Lett.* **115**, 120402 (2015).
- [47] E. T. Campbell, Decoherence in open Majorana systems, *Leibniz Int. Proc. Inform.* **44**, 111 (2015).
- [48] Y. Huang, A. M. Lobos, and Z. Cai, Dissipative Majorana quantum wires, *Science* **21**, 241 (2019).
- [49] C. Knapp, T. Karzig, R. M. Lutchyn, and C. Nayak, Dephasing of Majorana-based qubits, *Phys. Rev. B* **97**, 125404 (2018).
- [50] P. P. Aseev, J. Klinovaja, and D. Loss, Lifetime of Majorana qubits in Rashba nanowires with nonuniform chemical potential, *Phys. Rev. B* **98**, 155414 (2018).
- [51] P. P. Aseev, P. Marra, P. Stano, J. Klinovaja, and D. Loss, Degeneracy lifting of Majorana bound states due to electron-phonon interactions, *Phys. Rev. B* **99**, 205435 (2019).
- [52] O. Motrunich, K. Damle, and D. A. Huse, Griffiths effects and quantum critical points in dirty superconductors without spin-rotation invariance: One-dimensional examples, *Phys. Rev. B* **63**, 224204 (2001).
- [53] P. W. Brouwer, M. Duckheim, A. Romito, and F. von Oppen, Probability Distribution of Majorana End-State Energies in Disordered Wires, *Phys. Rev. Lett.* **107**, 196804 (2011).
- [54] P. W. Brouwer, M. Duckheim, A. Romito, and F. von Oppen, Topological superconducting phases in disordered quantum wires with strong spin-orbit coupling, *Phys. Rev. B* **84**, 144526 (2011).
- [55] A. R. Akhmerov, J. P. Dahlhaus, F. Hassler, M. Wimmer, and C. W. J. Beenakker, Quantized Conductance at the Majorana Phase Transition in a Disordered Superconducting Wire, *Phys. Rev. Lett.* **106**, 057001 (2011).
- [56] M.-T. Rieder, G. Kells, M. Duckheim, D. Meidan, and P. W. Brouwer, Endstates in multichannel spinless p -wave superconducting wires, *Phys. Rev. B* **86**, 125423 (2012).
- [57] M.-T. Rieder, P. W. Brouwer, and I. Adagideli, Reentrant topological phase transitions in a disordered spinless superconducting wire, *Phys. Rev. B* **88**, 060509(R) (2013).
- [58] W. DeGottardi, D. Sen, and S. Vishveshwara, Majorana Fermions in Superconducting 1D Systems Having Periodic, Quasiperiodic, and Disordered Potentials, *Phys. Rev. Lett.* **110**, 146404 (2013).
- [59] F. Pientka, A. Romito, M. Duckheim, Y. Oreg, and F. von Oppen, Signatures of topological phase transitions in mesoscopic superconducting rings, *New J. Phys.* **15**, 025001 (2013).
- [60] E. M. Stoudenmire, J. Alicea, O. A. Starykh, and M. P. A. Fisher, Interaction effects in topological superconducting wires supporting Majorana fermions, *Phys. Rev. B* **84**, 014503 (2011).
- [61] E. Sela, A. Altland, and A. Rosch, Majorana fermions in strongly interacting helical liquids, *Phys. Rev. B* **84**, 085114 (2011).
- [62] R. M. Lutchyn and M. P. A. Fisher, Interacting topological phases in multiband nanowires, *Phys. Rev. B* **84**, 214528 (2011).
- [63] A. M. Lobos, R. M. Lutchyn, and S. Das Sarma, Interplay of Disorder and Interaction in Majorana Quantum Wires, *Phys. Rev. Lett.* **109**, 146403 (2012).
- [64] F. Crépin, G. Zaránd, and P. Simon, Nonperturbative phase diagram of interacting disordered Majorana nanowires, *Phys. Rev. B* **90**, 121407(R) (2014).
- [65] F. Hassler and D. Schuricht, Strongly interacting Majorana modes in an array of Josephson junctions, *New J. Phys.* **14**, 125018 (2012).
- [66] R. Thomale, S. Rachel, and P. Schmitteckert, Tunneling spectra simulation of interacting Majorana wires, *Phys. Rev. B* **88**, 161103(R) (2013).
- [67] H. Katsura, D. Schuricht, and M. Takahashi, Exact ground states and topological order in interacting Kitaev/Majorana chains, *Phys. Rev. B* **92**, 115137 (2015).
- [68] N. M. Gergs, L. Fritz, and D. Schuricht, Topological order in the Kitaev/Majorana chain in the presence of disorder and interactions, *Phys. Rev. B* **93**, 075129 (2016).
- [69] D. J. Luitz, N. Laflorencie, and F. Alet, Many-body localization edge in the random-field Heisenberg chain, *Phys. Rev. B* **91**, 081103(R) (2015).
- [70] M.-C. Chung and I. Peschel, Density-matrix spectra of solvable fermionic systems, *Phys. Rev. B* **64**, 064412 (2001).
- [71] I. Peschel, Calculation of reduced density matrices from correlation functions, *J. Phys. A: Math. Gen.* **36**, L205 (2003).
- [72] I. Peschel, On the reduced density matrix for a chain of free electrons, *J. Stat. Mech.: Theory Exp.* **2004** P06004 (2004).
- [73] I. Peschel and V. Eisler, Reduced density matrices and entanglement entropy in free lattice models, *J. Phys. A: Math. Theor.* **42**, 504003 (2009).

- [74] J. M. Zhang and N. J. Mauser, Optimal Slater-determinant approximation of fermionic wave functions, *Phys. Rev. A* **94**, 032513 (2016).
- [75] N. Bray-Ali, L. Ding, and S. Haas, Topological order in paired states of fermions in two dimensions with breaking of parity and time-reversal symmetries, *Phys. Rev. B* **80**, 180504(R) (2009).
- [76] S. Gangadharaiyah, B. Braunecker, P. Simon, and D. Loss, Majorana Edge States in Interacting One-Dimensional Systems, *Phys. Rev. Lett.* **107**, 036801 (2011).
- [77] G. Goldstein and C. Chamon, Exact zero modes in closed systems of interacting fermions, *Phys. Rev. B* **86**, 115122 (2012).
- [78] G. Yang and D. E. Feldman, Exact zero modes and decoherence in systems of interacting Majorana fermions, *Phys. Rev. B* **89**, 035136 (2014).
- [79] G. Kells, Many-body Majorana operators and the equivalence of parity sectors, *Phys. Rev. B* **92**, 081401(R) (2015).
- [80] G. Kells, Multiparticle content of Majorana zero modes in the interacting p -wave wire, *Phys. Rev. B* **92**, 155434 (2015).
- [81] P. Fendley, Strong zero modes and eigenstate phase transitions in the XYZ/interacting Majorana chain, *J. Phys. A: Math. Theor.* **49**, 30LT01 (2016).
- [82] J. Kemp, N. Y. Yao, C. R. Laumann, and P. Fendley, Long coherence times for edge spins, *J. Stat. Mech.* **2017** (2017)063105.
- [83] M. McGinley, J. Knolle, and A. Nunnenkamp, Robustness of Majorana edge modes and topological order—exact results for the symmetric interacting Kitaev chain with disorder, *Phys. Rev. B* **96**, 241113(R) (2017).
- [84] J.-J. Miao, H.-K. Jin, F.-C. Zhang, and Y. Zhou, Exact Solution for the Interacting Kitaev Chain at the Symmetric Point, *Phys. Rev. Lett.* **118**, 267701 (2017).
- [85] A. S. Jermyn, R. S. K. Mong, J. Alicea, and P. Fendley, Stability of zero modes in parafermion chains, *Phys. Rev. B* **90**, 165106 (2014).
- [86] N. Moran, D. Pellegrino, J. K. Slingerland, and G. Kells, Parafermionic clock models and quantum resonance, *Phys. Rev. B* **95**, 235127 (2017).
- [87] D. Pellegrino, G. Kells, N. Moran, and J. K. Slingerland, Constructing edge zero modes through domain wall angle, *J. Phys. A: Math. Theor.* **53** 095006 (2020).
- [88] I. Mahyach and E. Ardonne, Study of the phase diagram of the Kitaev-Hubbard chain, *Phys. Rev. B* **101**, 085125 (2020).
- [89] D. V. Else, P. Fendley, J. Kemp and C. Nayak, Prethermal Strong Zero Modes and Topological Qubits, *Phys. Rev. X* **7**, 041062 (2017).
- [90] M. Rigol, V. Dunjko, V. Yurovsky, and M. Olshanii, Relaxation in a Completely Integrable Many-Body Quantum System: An *Ab Initio* Study of the Dynamics of the Highly Excited States of 1D Lattice Hard-Core Bosons, *Phys. Rev. Lett.* **98**, 050405 (2007).
- [91] M. Rigol, V. Dunjko, and M. Olshanii, Thermalization and its mechanism for generic isolated quantum systems, *Nature (London)* **452**, 854 (2008).
- [92] M. Kollar, F. A. Wolf, and M. Eckstein, Generalized Gibbs ensemble prediction of prethermalization plateaus and their relation to nonthermal steady states in integrable systems, *Phys. Rev. B* **84**, 054304 (2011).
- [93] A. C. Cassidy, C. W. Clark, and M. Rigol, Generalized Thermalization in an Integrable Lattice System, *Phys. Rev. Lett.* **106**, 140405 (2011).
- [94] C. Gogolin, M. P. Müller, and J. Eisert, Absence of Thermalization in Nonintegrable Systems, *Phys. Rev. Lett.* **106**, 040401 (2011).
- [95] L. Vidmar and M. Rigol, Generalized Gibbs ensemble in integrable lattice models, *J. Stat. Mech.* **2016** (2016)064007.
- [96] The eigenstate-thermalization hypothesis (ETH) is associated primarily with the applicability of equilibrium statistical mechanics to isolated quantum systems. In particular, for an isolated quantum system satisfying the ETH, in the thermodynamic limit the expectation values of few body operators in an initial state relax to the equilibrium thermal value set by the average energy of the initial state. In particular, given the thermalization of the system at a given temperature, for any subsystem, the rest of the system acts as a bath in which the reduced density matrix of the subsystem tends to the predicted equilibrium density matrix at the given temperature (see, e.g., [97]). This in particular infers a volume law scaling to the entanglement entropy of the subsystems. The ETH however does not hold for all isolated quantum systems. One example of this would be systems that are integrable systems. Another example is systems in what has been called a many-body localized (MBL) phase. The important ingredients for the MBL phase are the presence of disorder and interactions. It was shown by Anderson [98] that in noninteracting systems the presence of disorder causes localization in the single particle (Anderson) orbitals. The idea of localization in a many-body context arrived much later [99–106]. Features of the MBL phase include zero DC conductivity in the system, an area law entanglement for eigenstates, and a logarithmic spreading of entanglement from nonentangled initial conditions.
- [97] R. Nandkishore and D. A. Huse, Many-body localization and thermalization in quantum statistical mechanics, *Annu. Rev. Condens. Matter* **6**, 15 (2015).
- [98] P. W. Anderson, Absence of diffusion in certain random lattices, *Phys. Rev.* **109**, 1492 (1958).
- [99] I. V. Gornyi, A. D. Mirlin, and D. G. Polyakov, Interacting Electrons in Disordered Wires: Anderson Localization and Low- T Transport, *Phys. Rev. Lett.* **95**, 206603 (2005).
- [100] D. M. Basko, I. L. Aleiner, and B. L. Altshuler, Metal-insulator transition in a weakly interacting many-electron system with localized single-particle states, *Ann. Phys.* **321**, 1126 (2006).
- [101] V. Oganesyan and D. A. Huse, Localization of interacting fermions at high temperature, *Phys. Rev. B* **75**, 155111 (2007).
- [102] A. Pal and D. A. Huse, Many-body localization phase transition, *Phys. Rev. B* **82**, 174411 (2010).
- [103] J. H. Bardarson, F. Pollmann, and J. E. Moore, Unbounded Growth of Entanglement in Models of Many-Body Localization, *Phys. Rev. Lett.* **109**, 017202 (2012).
- [104] D. A. Huse, R. Nandkishore, and V. Oganesyan, Phenomenology of fully many-body-localized systems, *Phys. Rev. B* **90**, 174202 (2014).
- [105] S. Bera, H. Schomerus, F. Heidrich-Meisner, and J. H. Bardarson, Many-Body Localization Characterized from a One-Particle Perspective, *Phys. Rev. Lett.* **115**, 046603 (2015).
- [106] S. Bera, T. Martynek, H. Schomerus, F. Heidrich-Meisner, and J. H. Bardarson, One-particle density matrix characterization

- of many-body localization, *Ann. Phys. (Berlin)* **529**, 1600356 (2017).
- [107] W. Beugeling, A. Andreanov, and M. Haque, Global characteristics of all eigenstates of local many-body Hamiltonians: Participation ratio and entanglement entropy, *J. Stat. Mech.* **2015** (2015)P02002.
- [108] J.-P. Blaizot and G. Ripka, *Quantum Theory of Finite-Systems* (MIT Press, Cambridge, MA, 1986), pp. 34–38 and 101–103.
- [109] See the Supplemental Material at <http://link.aps.org/supplemental/10.1103/PhysRevB.102.054508> for videos (.avi files) displaying the entropy-energy plots for fixed values U and increasing disorder strength.